frontiers in Pharmacology

ORIGINAL RESEARCH
published: 16 September 2021
doi: 10.3389/fphar.2021.720685

Andrographolide Sulfonate Is a Promising Treatment to Combat Methicillin-resistant *Staphylococcus aureus* and Its Biofilms

Lulu Zhang[1,2†], Bo Wen[1†], Mei Bao[1,2], Yungchi Cheng[3], Tariq Mahmood[4], Weifeng Yang[5], Qing Chen[1,2], Lang Lv[6], Li Li[1], Jianfeng Yi[2], Ning Xie[6], Cheng Lu[1] and Yong Tan[1]**

[1]Institute of Basic Research in Clinical Medicine, China Academy of Chinese Medical Sciences, Beijing, China, [2]Key Laboratory for Research on Active Ingredients in Natural Medicine of Jiangxi Province, Yichun University, Yichun, China, [3]Department of Pharmacology, Yale University School of Medicine, New Haven, CT, United States, [4]Department of Plant Sciences, Faculty of Biological Sciences, Quaid-i-Azam University, Islamabad, Pakistan, [5]Medical Experimental Center, China Academy of Chinese Medical Sciences, Beijing, China, [6]Qingfeng Pharmaceutical Co. Ltd., Ganzhou, China

OPEN ACCESS

Edited by:
Priyia Pusparajah,
Monash University Malaysia, Malaysia

Reviewed by:
Appadurai Muthamil Iniyan,
Manonmaniam Sundaranar University, India
Khalid Mehmood,
Islamia University of Bahawalpur, Pakistan

***Correspondence:**
Cheng Lu
lv_cheng0816@163.com
Yong Tan
tcmtanyong@126.com

[†]These authors share first authorship

Specialty section:
This article was submitted to Ethnopharmacology, a section of the journal Frontiers in Pharmacology

Received: 04 June 2021
Accepted: 29 July 2021
Published: 16 September 2021

Citation:
Zhang L, Wen B, Bao M, Cheng Y, Mahmood T, Yang W, Chen Q, Lv L, Li L, Yi J, Xie N, Lu C and Tan Y (2021) Andrographolide Sulfonate Is a Promising Treatment to Combat Methicillin-resistant Staphylococcus aureus and Its Biofilms. Front. Pharmacol. 12:720685. doi: 10.3389/fphar.2021.720685

Methicillin-resistant *Staphylococcus aureus* (MRSA) is a drug-resistant pathogen threatening human health and safety. Biofilms are an important cause of its drug resistance and pathogenicity. Inhibition and elimination of biofilms is an important strategy for the treatment of MRSA infection. Andrographolide sulfonate (AS) is an active component of the traditional herbal medicine *Andrographis paniculata*. This study aims to explore the inhibitory effect and corresponding mechanisms of AS on MRSA and its biofilms. Three doses of AS (6.25, 12.5, and 25 mg/ml) were introduced to MRSA with biofilms. *In vitro* antibacterial testing and morphological observation were used to confirm the inhibitory effect of AS on MRSA with biofilms. Real-time PCR and metabonomics were used to explore the underlying mechanisms of the effect by studying the expression of biofilm-related genes and endogenous metabolites. AS displayed significant anti-MRSA activity, and its minimum inhibitory concentration was 50 μg/ml. Also, AS inhibited biofilms and improved biofilm permeability. The mechanisms are mediated by the inhibition of the expression of genes, such as quorum sensing system regulatory genes (*agrD* and *sarA*), microbial surface components–recognizing adhesion matrix genes (*clfA* and *fnbB*), intercellular adhesion genes (*icaA*, *icaD,* and *PIA*), and a gene related to cellular eDNA release (*cidA*), and the downregulation of five biofilm-related metabolites, including anthranilic acid, *D*-lactic acid, kynurenine, *L*-homocitrulline, and sebacic acid. This study provided valuable evidence for the activity of AS against MRSA and its biofilms and extended the methods to combat MRSA infection.

Keywords: andrographolide sulfonate, methicillin-resistant *Staphylococcus aureus*, drug-resistant biofilm, RT-PCR, metabonomics

INTRODUCTION

Methicillin-resistant *Staphylococcus aureus* (MRSA) is one of the most common drug-resistant bacteria, and MRSA infection has posed a serious threat to public health (Fulaz et al., 2020). The formation of MRSA biofilms and their inherent resistance to antibiotics is the root cause of MRSA infection (Zhang et al., 2020). Biofilms are an organized bacterial population that gradually forms during an infection and have the ability to withstand antibiotics (Craft et al., 2019; Cascioferro et al., 2021). A positive relationship has generally been observed between biofilm formation ability and antimicrobial resistance (Sun et al., 2019). Bacteria that attach to a surface and grow as biofilms are protected from antibiotic-induced killing. In addition, reduced antibiotic susceptibility contributes to the persistence of biofilm infections, forming a vicious cycle (Feng et al., 2020). This result explains why MRSA has acquired resistance to practically all antibiotics developed for clinical use in the past 50 years, including vancomycin (Van), which is the last resort to treating MRSA infection (Howden et al., 2010; McGuinness et al., 2017). Researchers have turned their attention to traditional medicine (TM), expecting to identify potential antibacterial drugs that will address the limitation that all antibiotics, including Van, are ineffective at removing mature biofilms (Chopra et al., 2015).

TM mainly originates from natural products. TM exerts its effect through different mechanisms compared to conventional antibiotics, which might be of clinical value in the treatment of infectious diseases associated with biofilms (Ordonez et al., 2011; Borges et al., 2015). *Andrographis paniculata*, a highly abundant natural product and medicinal plant, is regarded as a "natural antibiotic" (Patil and Jain, 2020). Pharmacological studies have shown that it possesses anti-inflammatory, antibacterial, and antipyretic properties (Patil and Jain, 2020) and it has been used to treat a variety of infectious diseases, such as furuncle, upper respiratory tract infection, and chronic pharyngitis caused by MRSA infection. The antibacterial activity is primarily attributed to andrographolide (AG), the active constituent of the herb (Liew et al., 2020). AG exhibits potential antibacterial activity against most Gram-positive bacteria, among which MRSA is the most sensitive to AG (Banerjee et al., 2017). More importantly, AG significantly inhibits biofilm formation without cytotoxicity (Feng et al., 2020). It works by inhibiting virulence factors and the quorum sensing (QS) system, an intercellular communication mechanism closely related to biofilm formation, stability, and development (Solano et al., 2014; Castillo-Juarez et al., 2015). According to previous studies, andrographolide sulfonate (AS), a water-soluble form of silver sulfonate, is the main ingredient in Xiyanping injection. It is more effective in inhibiting bacterial growth and the QS system than the parental compound AG (Zhang et al., 2019a). Xiyanping injection has also long been used in the clinic to treat community-acquired pneumonia, and, compared with azithromycin, it performs better in terms of clinical indicators, such as shorter hospital stays, reduced adverse effects, and time to lung-shadow absorption assessment (Shi et al., 2019). Nevertheless, to date, the specific pharmacodynamic mechanism of AS against MRSA is not known. Therefore, elucidating the therapeutic effect of AS on MRSA infection and the mechanism underlying its efficacy is important for further research on the antibacterial activity of AS.

In the study of drug interventions for MRSA biofilms, choosing the right methodology will provide an important support and ensure the reliability and credibility of the study. Real-time PCR (RT-PCR) is a commonly used method for quantitative analyses of gene expression. In recent years, it has become a standard tool for many laboratories and scientists working in the field of microbial ecology to determine the pathway and characteristics of drug action (Thomas et al., 2012). Metabolomics, an important branch of systematic biology, is mainly used to evaluate the effects of the environment, disease status, or drug intervention on endogenous small-molecule metabolites, such as amino acids, peptides, and lipids (Zhang et al., 2018). It adopts a "top-down" strategy to reflect the function of organisms from terminal symptoms of metabolic networks and understand metabolic changes in a complete system caused by interventions in a holistic context (Wang X. et al., 2011). Metabolomics covers a wide range of substances and focuses on holistic and dynamic evaluation (Zhang et al., 2018), beneficially providing an opportunity to scientifically examine the treatment effect of TM (Wang X. et al., 2011). Recently, metabolomics investigations have been widely used to evaluate the biological efficacy and corresponding mechanism of TM.

In the present study, *in vitro* antibacterial experiments and morphological observations were used to determine the effects of AS on MRSA biofilms. Based on these confirmed effects, RT-PCR was applied to elucidate the expression of biofilm-related genes. Additionally, metabolomics testing was performed to identify novel biomarkers capable of characterizing mature MRSA biofilms and the pharmaceutical mechanism of AS. This study preliminarily elucidated the inhibitory effect and corresponding mechanism of AS on MRSA and MRSA biofilms, which provides valuable evidence and guidance for the clinical diagnosis and therapy of MRSA infection.

METHODS

Antimicrobial Agents and Chemicals

AS was provided by Jiangxi Qingfeng Pharmaceutical Co., Ltd. (Ganzhou, China). Van hydrochloride injection (lot no. 657) was obtained from EliLilly, Japan. Tryptone and yeast extracts were obtained from Oxoid, United Kingdom, NaCl was obtained from Merck, Germany, and 2,3,5-triphenyltetrazolium chloride (TTC) was obtained from Amresco, United States. 2,3-Bis-(2-methoxy-4-nitro-5-sulfophenyl)-2H-tetrazolium-5-carboxanilide (XTT) and phenazine methosulfate (PMS) were purchased from Sigma-Aldrich, United States.

Strains and Growth Conditions

MRSA was obtained from samples of MRSA strains that had been identified and isolated in the Laboratory Department of Dongzhimen Hospital in Beijing. MRSA was maintained in

cryogenic storage at −80°C on glass beads. Working cultures of bacteria were maintained on the solid LB medium at 4°C and subcultured in the liquid LB medium. In brief, the MRSA strain was cultured with shaking at 280 rpm for 18 h at 37°C and diluted with the LB medium to the starting inoculum with an OD_{600} = 0.02.

Determination of the Minimum Inhibitory Concentration

The minimum inhibitory concentration (MIC) is defined as the lowest sample concentration that completely inhibits the growth of microorganisms (Fankam et al., 2011). The MIC of AS for MRSA was determined using the microbroth dilution method. The experiment was performed in sterile 96-well plates in a final volume of 200 μl, consisting of 100 μl of microbial cultures (OD_{600} = 0.02) and 100 μl of serially diluted AS (0.1, 0.2, 0.78, 1.56, 3.13, 6.25, 12.5, 25, and 50 mg/ml). Van (0.25, 0.5, 1, 2, 4, 8, 16, 32, 64, and 128 μg/ml) was used as a positive control drug. Microplates were incubated at 37°C for 24 h, followed by the addition of 20 μl of 2.5 mg/ml TTC and incubation for an additional 20 min at 37°C. Viable bacteria reduced the yellow dye to pink.

Biofilm Assays

The method for biofilm quantification was performed as described previously and modified as described by Wang Y. et al., 2011. We used the LB medium containing 0.25% glucose (LB-G) to dilute the MRSA bacterial solution to an OD_{600} = 0.1. The diluted culture was transferred to a sterile 96-well plate and incubated at 37°C and 80% RH for 24 h. One hundred microliters of AS (6.25, 12.5, and 25 mg/ml) was added, and the well containing the medium was used as a negative control well. After incubating the cultures at 37°C and 80% RH for 24 h, the medium and planktonic cells were removed and the wells containing the biofilm were washed with 0.9% NaCl. Then, the XTT reduction assay was performed to evaluate the viability of the biofilms. For this experiment, 40 μl of the XTT-PMS mixed solution (XTT:PMS = 1:100) was added to each well. The 96-well plate was incubated in the dark at 37°C for 20 min, and then, the optical density was measured at 490 nm using a microplate reader. A decrease in the number of live cells correlates with a decrease in the overall activity of the dehydrogenases responsible for transforming the sodium salt of XTT into formazan, which was determined colorimetrically (Yang et al., 2018).

Confocal Laser Scanning Microscopy

MRSA (OD_{600} = 0.1) diluted with LB-G was transferred to a sterile Petri dish and incubated at 37°C and 80% RH for 24 h. After the planktonic bacteria were removed, 1 ml of 25 mg/ml AS and 4 μg/ml Van were added and LB-G was used as a negative control. After incubating at 37°C and 80% RH for 24 h, the supernatant was removed. Three fluorescent dyes were used for staining. SYTO-9 and PI from the LIVE/DEAD®BacLight™ Bacterial Viability Kit (cat. no. L7012) and Matrix-staining solution were used to measure the extracellular matrix of biofilms. The ratio of the three dye solutions was 1.5:1.5:1,000. The biofilm was stained in the dark for 20 min. Then, the dye was removed, and 500 μl of LB-G was added to each well. The tomographic images, three-dimensional reconstruction images, and images of the biofilm thickness were captured using an Olympus TM FluoView FV1000 microscope to determine the spatial distribution of living/dead bacteria in the biofilm structure. The samples were placed under a confocal laser scanning microscope and observed with a ×10 objective at the different excitation wavelengths of SYTO-9 (488 nm), PI (559 nm), and Matrix (559 nm) stains. SYTO-9 quickly penetrates the cell wall and binds to DNA with green fluorescence; therefore, it characterizes living bacteria. On the other hand, PI does not penetrate the intact cell wall but binds to the mixture of damaged cell DNA and extracellular DNA with red fluorescence to characterize the dead bacteria.

Scanning Electron Microscopy

The biofilm samples were prepared on glass cover slides using the method described above. The sample was fixed with 4% glutaraldehyde for 24 h at 4°C and then fixed with 1% osmic acid for 1 h. After gradual dehydration with ethyl alcohol solutions (60, 70, 80, 90, 95, and 100%), the sample was freeze-dried. The specimens were then sputter-coated with gold. Finally, the cells were observed under a scanning electron microscope.

Detection of Biofilm Permeability

The change in biofilm permeability was judged by observing the change in the size of the bacteriostatic zone caused by the filter paper with the increase in the time required to absorb Van from agar plates covered by biofilms. The change in the permeability of MRSA biofilms treated with AS and Van was detected by establishing a filter paper–biofilm–antibiotic agar plate model (Anderl et al., 2000). MRSA biofilms were cultured on round aseptic paper in the LB-G medium and incubated with 12.5 mg/ml AS, 25 mg/ml AS, or 4 μg/ml Van for 24 h. At the same time, the LB-G medium was used as a negative control group. The treated biofilm was transferred to an LB agar plate containing 500 μg/ml Van, and a round 6 mm wet filter paper was placed on the biofilm. If the biofilm structure is destroyed, the Van from the agar plate will be adsorbed on the filter paper according to the permeation principle. After incubating at 37°C and 80% RH for 2, 4, and 6 h, the round filter paper was transferred to an LB agar plate covered with MRSA. The size of the bacteriostatic zone was measured after incubating at 37°C and 80% RH for 18 h.

Detection of the Expression of MRSA Biofilm–Related Genes Using Real-Time PCR

Extraction of Total RNA

The relative quantitative analysis of gene expression in planktonic MRSA and mature MRSA biofilms was carried out using RT-PCR. MRSA cells were cultured with LB-G at 37°C and 280 rpm for 0 and 24 h, respectively, and then incubated with 25 mg/ml AS at 37°C and 80% RH for 24 h. The cells were then harvested by centrifugation and immediately suspended in RNAlater

TABLE 1 | Primer sequences used for the quantitative analysis.

Primer name	Primer sequence (5′→3′)	Accession number
agrD-F	TCATTTTTTGATTTTATAACTGGTG	AF288215.1
agrD-R	TCTTTAGGTATTTCAACTTCGTCC	
cidA-F	TAACTTGGGTAGAAGACGGTGC	NC_022604
cidA-R	CGTCTACACCTTTACGATGTTTATG	
clfA-F	ATTGGCGTGGCTTCAGTGCT	CP076105.1
clfA-R	CGTTTCTTCCGTAGTTGCATTTG	
fnbB-F	AGGAAGAAGCGAAACCTCAAG	CP076105
fnbB-R	ATGCCCCTCAATAGAACCAAT	
icaA-F	CGAAGTCAGACACTTGCTGG	CP076105.1
icaA-R	GCTTCCAAAGACCTCCCAA	
icaD-F	GGTCAAGCCCAGACAGAGG	CP076027.1
icaD-R	ACACACGATATAGCGATAAGTGC	
PIA-F	CCTATCCTTATGGCTTGATGAAT	NC_007795.1
PIA-R	TAATAATCATTGGAGTTCGGAGTG	
sarA-F	ATGGGGAACATGATCCTTTG	CP076105.1
sarA-R	TAGCCGCATAACGAGCAGTA	
16S rRNA-F	TTCTGGTCTGTAACTGACGCTG	CP071594.1
16S rRNA-R	CGAAGGGGAAGGCTCTATCT	

(Ambion, Austin, TX). RNA was then purified with the SV Total RNA Isolation system (Promega, Madison, WI), followed by DNaseI treatment (Turbo DNA-free kit; Ambion) to eliminate residual contamination of genomic DNA. The purity and concentration of the RNA were determined by spectrophotometry and gel electrophoresis. Reverse transcription reactions were performed with the High-Capacity Complementary DNA (cDNA) Reverse Transcription Kit (ABI, Foster City, CA).

Real-Time PCR

PCR primers (**Table 1**) were designed with Primer Express Software Version 3.0 (ABI). Amplification of cDNA (1 ng) was performed with 250 nM gene-specific primers and a PowerSYBR Green Master Mix (ABI). PCR amplification, detection, and analyses were performed using the StepOne RT-PCR system (ABI). The critical threshold cycle was defined for each sample, and expression levels were normalized to the 16S rRNA gene as an internal standard; 16S rRNA levels did not vary under our experimental conditions. Each assay was performed in triplicate.

UPLC-TOF-MS Detection of Metabolites in MRSA Biofilms

Metabonomics Sample Preparation

Nontargeted metabonomics was conducted, and the mechanism underlying the effect of 25 mg/ml AS on MRSA was discussed. Twenty-five millilitres of a MRSA solution with an OD_{600} = 0.1 was added to two sterile 250 ml conical flasks. An overnight biofilm culture was prepared by incubating the sample in a constant-temperature concussion box at 37°C and 180 rpm for 24 h. The AS (25 mg/ml) and blank LB medium (50 ml) were added to the conical flask on the next day. Fifty milliliters of the MRSA cultures at an OD_{600} = 0.1 and the same volume of blank LB medium were added to another conical flask. After 24 h of coincubation, the same volume of 60% methanol in water was added at −20°C for cold methanol extraction. The sample was centrifuged at 3,000 rpm for 10 min at 4°C. Then, the supernatant was removed, and the precipitate was stored at −80°C until metabolite extraction.

Extraction and Analysis of Metabolites

After thawing at room temperature, 300 µl of methanol was added to the sample. Proteins were precipitated with methanol, fully swirled for 30 s, and centrifuged at 12,000 rpm for 15 min at 4°C. An equal volume of each sample was combined and used as a quality control (QC) sample.

The instrument analysis platform was LC-Q/TOF-MS (Agilent, 1290 Infinity LC, 6545 UHD, and Accurate-Mass Q-TOF/MS), and the separation column was a C18 column (Agilent, 100 mm × 2.1 mm, 1.8 µm). The chromatographic separation conditions are described as follows. The column temperature was 40°C. The flow rate was 0.4 ml/min. The mobile phase consisted of A, water+0.1% formic acid, and B, acetonitrile+0.1% formic acid. The injection volume was 4 µl, and the temperature of the automatic injector was 4°C. The LC/MS data were preprocessed using Mass Profiler software (Agilent) and edited later in EXCEL2007 software. The final results were organized into a two-dimensional data matrix, including variables (retention time and mass-to-charge ratio), observation quantity (sample), and peak intensity.

The edited data matrix was imported into SIMCA-P software (Umetrics AB, Umea, Sweden, version 13.0) for principal component analysis (PCA). Statistical analyses were performed using the free online tool MetaboAnalyst 3.0. In brief, the exported table of putative metabolites with a median RSD of <0.2 (20%) within the QC group and a confidence level of >5 was uploaded to MetaboAnalyst 3.0. Data with >50% missing values were removed, and the remaining missing values were replaced with a small value (half the minimum positive value in the original data) (Wehrens and Salek, 2016). Data were filtered using the interquartile range, normalized to the median, log2 transformed, and autoscaled (mean centered and divided by the standard deviation of each variable). One-way ANOVA and Fisher's least square difference (LSD) test were used to identify the significantly perturbed metabolites between the 25 mg/ml AS-treated and control groups. Statistically and significantly altered metabolites were selected using a false discovery rate of <0.05 for one-way ANOVA and a p value of <0.05 for Fisher's LSD test.

RESULTS

Antibacterial Activity of Andrographolide Sulfonate and Vancomycin Against MRSA

MRSA strains have different sensitivity rates to AS and Van. As shown in **Figure 1A**, Van exerted a bacteriostatic effect on MRSA at 4 µg/ml, AS had no bactericidal activity in the dose range of 0.1–25 mg/ml, and 50 mg/ml AS exerted the same inhibitory effect on MRSA as 4 µg/ml Van. The MIC of AS for MRSA is 50 mg/ml.

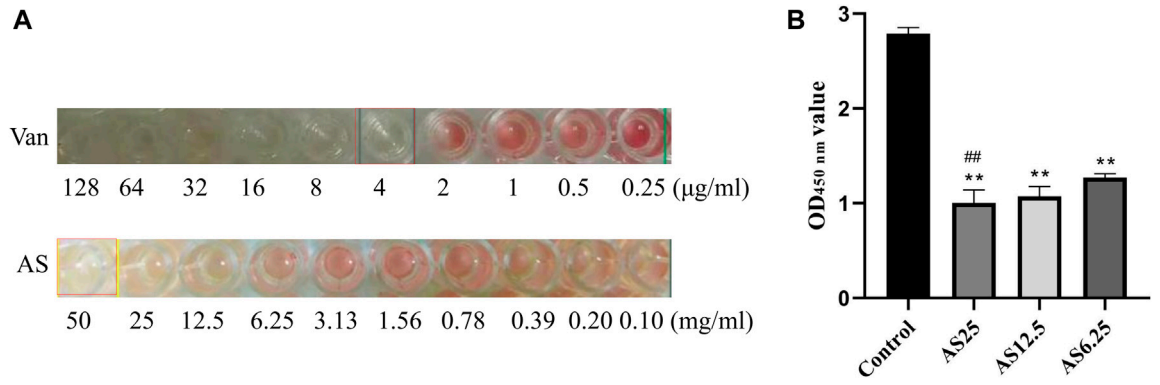

FIGURE 1 | Detection of the MIC of each drug for MRSA biofilms. **(A)** The MICs of Van and AS for MRSA. **(B)** Effects of different concentrations of AS on living bacteria in MRSA biofilms (**$p < 0.01$, compared with the control).

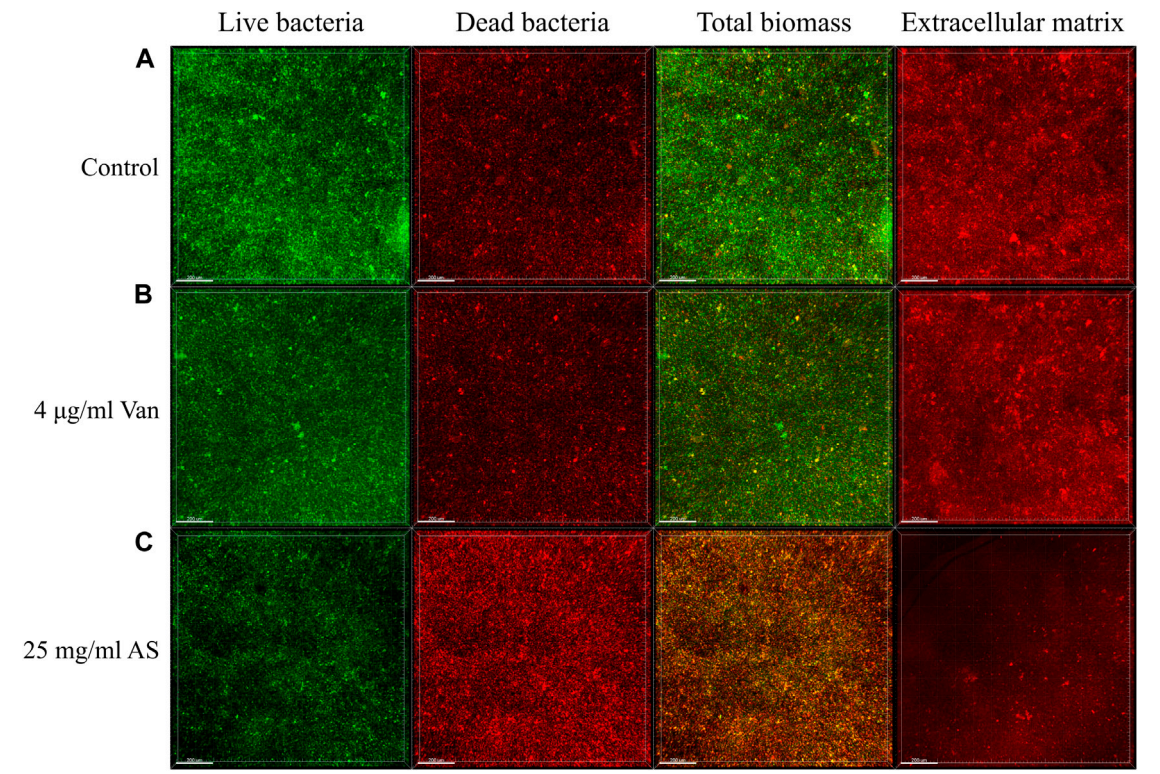

FIGURE 2 | CLSM micrographs of MRSA biofilms treated with AS and Van. In the first three columns, green represents the fluorescence signal of living bacteria and red represents the fluorescence signal of dead bacteria. The total biomass is the superposition of the two fluorescence signals, which indicates the corresponding biomass distribution of living bacteria and dead bacteria. The fourth column shows the distribution of the extracellular matrix fluorescence signal. The scale bar in images represents 200 μm.

Andrographolide Sulfonate Inhibits MRSA Biofilm Formation

Based on the MIC results of AS, three concentrations of AS, 1/8 MIC, 1/4 MIC, and 1/2 MIC (6.25, 12.5, and 25 mg/ml), were selected for the XTT reduction assay on MRSA biofilms. Compared with the untreated control biofilm, the effect on inducing biofilm cell death was stronger as the dose of AS increased (**Figure 1B**). The concentration of AS that produced the best inhibitory effect was 25 mg/ml. This concentration was used as the dose in our subsequent experiments.

Confocal laser scanning microscopy (CLSM) observations and digital image analysis showed that the surface of the control group

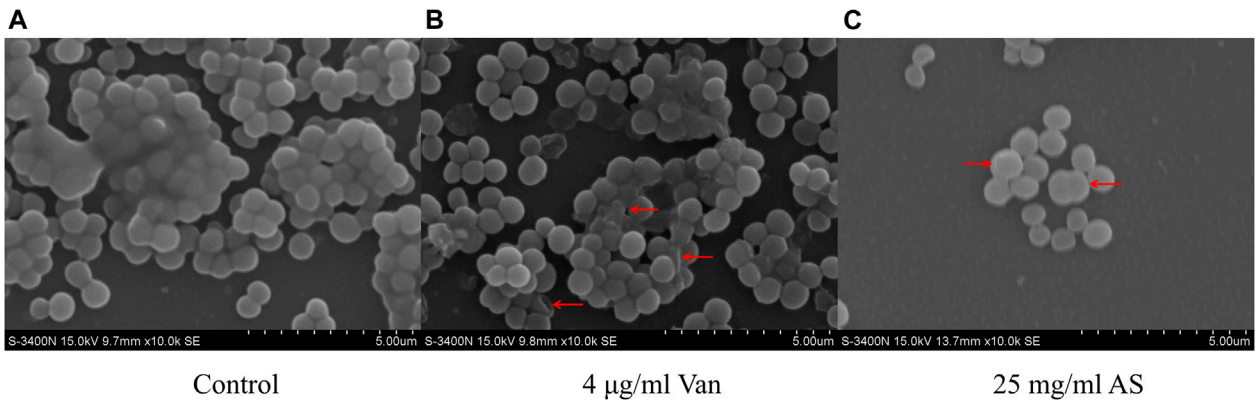

FIGURE 3 | SEM micrographs of MRSA biofilms treated with AS and Van. **(A)** Normal MRSA biofilms. **(B)** Abnormally shaped cells indicated by red arrows. **(C)** Cells with abnormal division indicated by a red arrow.

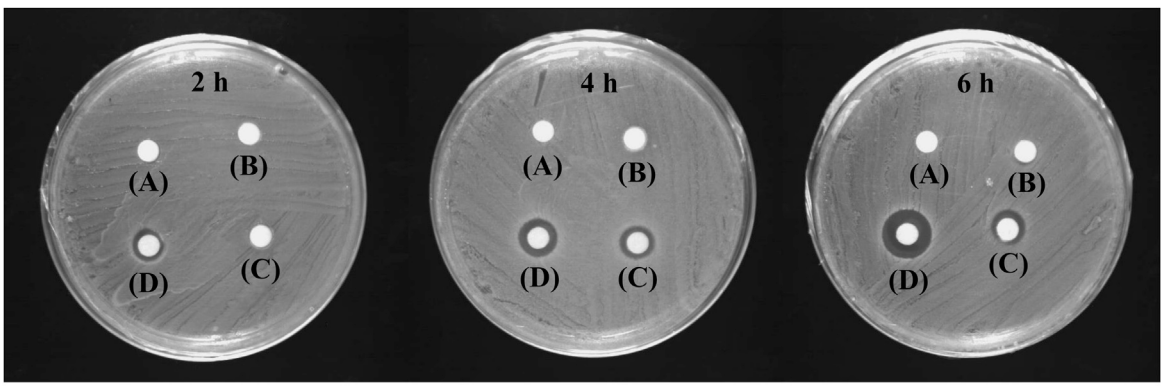

FIGURE 4 | Effects of AS and Van on the permeability of MRSA biofilms. The 16 μg/ml Van-treated group was the same as control group at all three time points and there was no inhibition zone. The 12.5 mg/ml AS showed inhibition zone at 4 h and 6 h, which was weak. The inhibition zone increased with an increasing duration of action of 25 mg/ml AS (6 h > 4 h > 2 h).

was rough, the fluorescence signal of living bacteria was strong, and the whole Petri dish was covered with many vigorous microbial colonies (**Figure 2**). The condition of the 4 μg/ml Van-treated group was similar to that of the control group. The fluorescence signal of living bacteria in the culture containing 25 mg/ml AS was weaker, and the number of colonies was substantially reduced. In addition, the fluorescence signal of dead bacteria was much higher than that of the former two groups. By staining the extracellular matrix with a Matrix-staining kit, the extracellular matrix content of the MRSA biofilm treated with 25 mg/ml AS was significantly lower than that of the 4 μg/ml Van-treated group. AS reduced the extracellular matrix content and inhibited the growth of living bacteria in the biofilm.

Scanning electron microscopy (SEM) observations at ×10000 magnification revealed that the biofilm structure of the control group was dense and massive colonies were growing on glass cover slips (**Figure 3**). The size of the cells was uniform, the shape was normal, and the surface was smooth. When MRSA was treated with 4 μg/ml Van, the structure of the biofilm was not as dense as that of the control group. Individual bacteria were damaged and presented an empty shell state after the outflow of the intracellular material. The structure of the biofilm almost completely disappeared in the electron microscopy image of the 25 mg/ml AS-treated group. Abnormal dichotomy and an increase in the volume were observed in the bacteria.

Effects of Vancomycin and Andrographolide Sulfonate on the Permeability of MRSA Biofilms

In the control group, no inhibition zone was observed at 2, 4, and 6 h, indicating that the biofilm permeability was low without drug intervention. No inhibition zone was detected in the 16 μg/ml

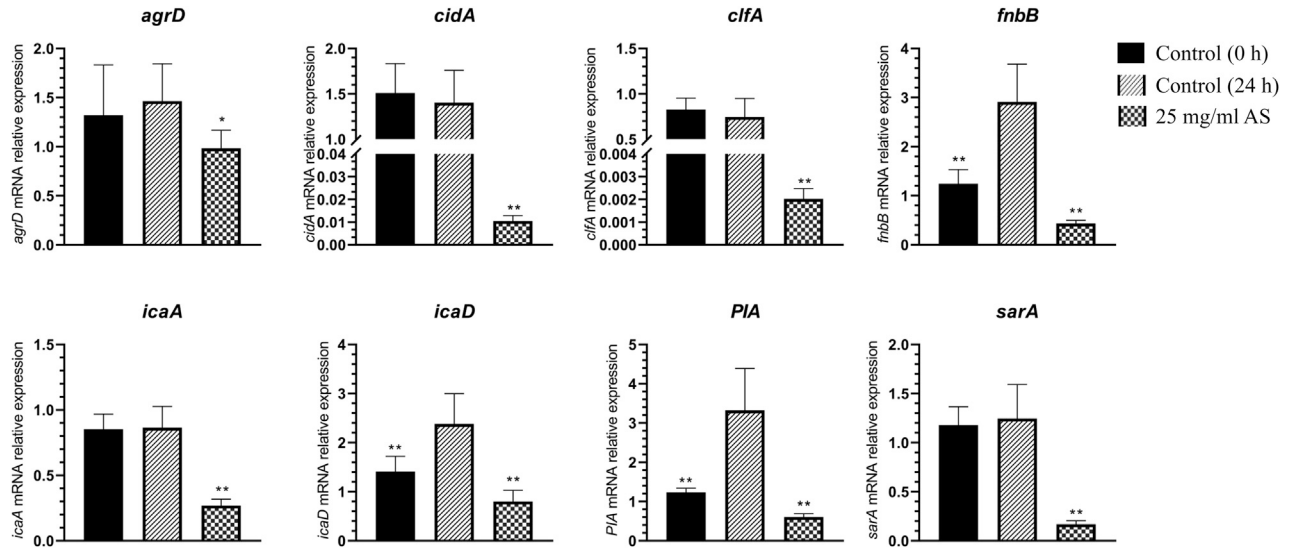

FIGURE 5 | Changes in MRSA gene expression. *$p < 0.05$, compared with the control (24 h); **$p < 0.01$, compared with the control (24 h).

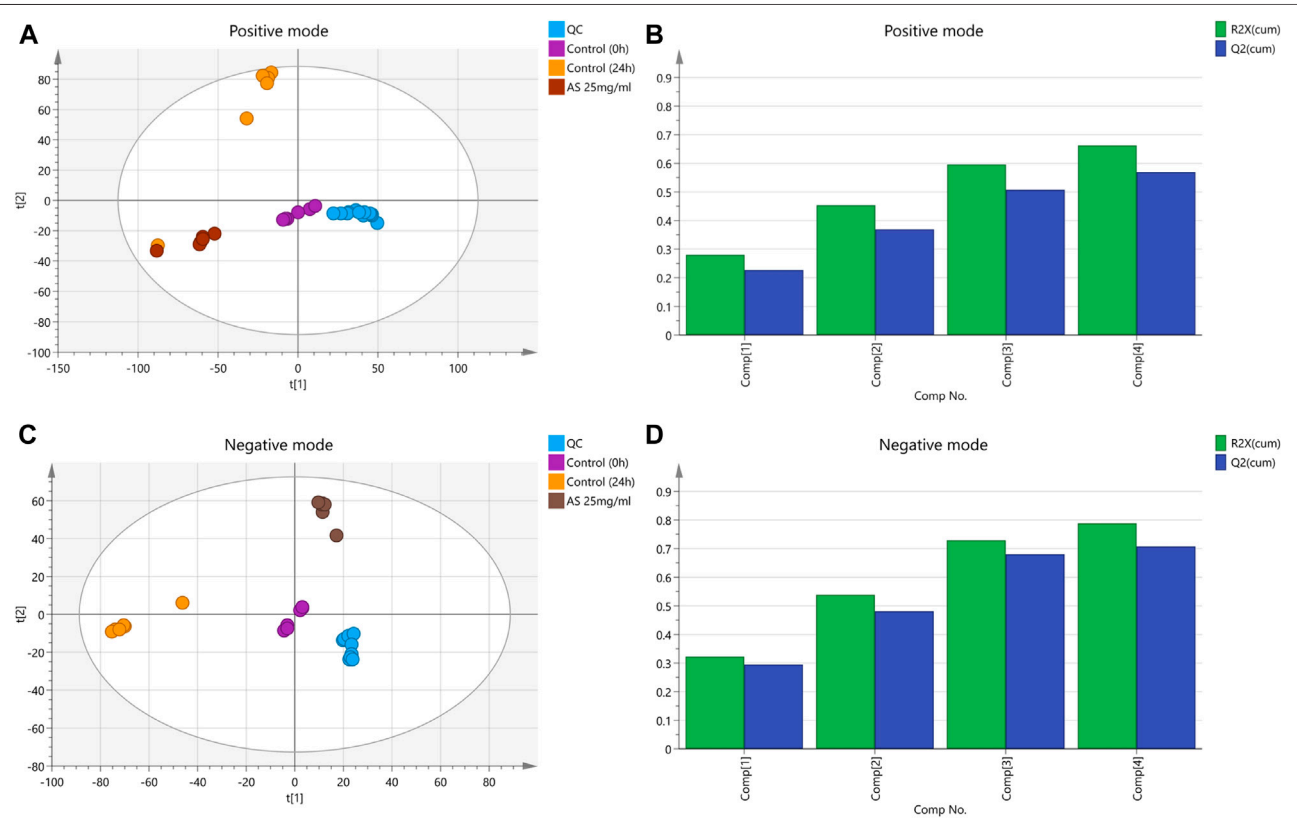

FIGURE 6 | PCA score plots based on the MRSA endogenous metabolic spectra obtained in the positive and negative ion mode. **(A** and **C)** PCA score plots; QC: quality control. **(B)** R2X = 0.663 cum, Q2 = 0.569 cum. **(D)** R2X = 0.788 cum, Q2 = 0.707 cum.

Van-treated group, which indicates that Van did not change the permeability of MRSA biofilms. However, 12.5 mg/ml AS produced an inhibition zone after 4 h and 25 mg/ml AS produced an inhibition zone after 2 h. Thus, AS improved the permeability of MRSA biofilms, and this effect occurred faster with increase in concentrations (**Figure 4**).

TABLE 2 | Characterization of terminal metabolites in MRSA biofilms.

n	RT (min)	Exact mass	Formula	Compound	KEGG	Fold change
1	5.96	210.0753	$C_8H_{10}N_4O_3$	1,3,7-Trimethyluric acid	C16361	5.925
2	1.1	891.204	$C_{29}H_{48}N_7O_{17}P_3S$	2E-Octenoyl-CoA	C05276	–6.914
3	5.36	851.1727	$C_{26}H_{44}N_7O_{17}P_3S$	2-Methylbutyryl-CoA	C01033	7.369
4	1.09	971.1575	$C_{32}H_{44}N_7O_{20}P_3S$	2-Succinylbenzoyl-CoA	C03160	–7.372
5	4.74	160.0974	$C_7H_{13}NO_3$	3-Dehydrocarnitine	C02636	–9.932
6	0.9	139.9875	$C_2H_5O_5P$	Acetyl phosphate	C00227	10.32
7	0.67	559.0717	$C_{15}H_{23}N_5O_{14}P_2$	ADP-ribose	C00301	–5.387
8	0.79	137.0477	$C_7H_7NO_2$	Anthranilic acid	C00108	6.859
9	1.75	329.0525	$C_{10}H_{12}N_5O_6P$	cAMP	C00575	4.493
10	0.84	111.0433	$C_4H_5N_3O$	Cytosine	C00380	–6.288
11	0.73	103.0633	$C_4H_9NO_2$	D-2-Aminobutyric acid	C02261	–4.792
12	0.71	307.0569	$C_9H_{14}N_3O_7P$	dCMP	C00239	6.882
13	0.72	90.0317	$C_3H_6O_3$	D-Lactic acid	C00256	4.197
14	0.73	147.0532	$C_5H_9NO_4$	Glutamate	C00025	–7.229
15	0.76	111.0796	$C_5H_9N_3$	Histamine	C00388	–3.219
16	4.84	208.0848	$C_{10}H_{12}N_2O_3$	Kynurenine	C01718	3.41
17	0.76	180.0634	$C_7H_{14}O_5$	*L*-(-)Sorbose	C00247	3.127
18	0.77	161.1052	$C_7H_{15}NO_3$	*L*-Carnitine	C00318	–4.065
19	6.99	189.1113	$C_7H_{15}N_3O_3$	*L*-Homocitrulline	C02427	3.616
20	1.13	181.0739	$C_9H_{11}NO_3$	*L*-Tyrosine	C00082	5.083
21	4.7	594.3417	$C_{33}H_{46}N_4O_6$	*L*-Urobilin	C05793	3.156
22	5.54	207.0895	$C_{11}H_{13}NO_3$	N-Acetyl-D-phenylalanine	C05620	4.615
23	1.14	164.0473	$C_9H_8O_3$	Phenylpyruvic acid	C00166	7.009
24	0.85	129.0426	$C_5H_7NO_3$	Pyroglutamic acid	C01879	–7.133
25	0.9	202.1205	$C_{10}H_{18}O_4$	Sebacic acid	C08277	3.932
26	1.07	342.1162	$C_{12}H_{22}O_{11}$	Sucrose	C00089	6.765
27	0.75	205.0375	$C_{10}H_7NO_4$	Xanthurenic acid	C02470	11.37

Effect of Andrographolide Sulfonate on MRSA Gene Expression

The expression of the adhesion-related genes, intercellular adhesion (*ica*) *D*, fibronectin binding (*fnb*) *B,* and polysaccharide intercellular adhesion (*PIA*), was significantly increased in MRSA biofilms, suggesting that these genes are closely associated with MRSA biofilm formation (**Figure 5**). When the mature MRSA biofilm was treated with 25 mg/ml AS, the expression of these genes was significantly inhibited compared with that of the control (24 h) (**Figure 5**).

The expression of staphylococcal accessory regulator (*sar*) *A* ($p < 0.01$) and accessory gene regulator (*agr*) *D* ($p < 0.05$) related to the QS system was downregulated to different degrees. The expression of *icaA*, clumping factor (*clf*) *A,* and *cidA* was also significantly downregulated after treatment with 25 mg/ml AS ($p < 0.01$).

Principal Component Analysis

In this analysis, 5 principal components were obtained in the positive mode, with R2X = 0.663 and Q2 = 0.569. In the negative mode, 8 principal components were obtained, with R2X = 0.788 and Q2 = 0.707. The PCA score chart is shown in **Figure 6**. Samples from the control group at 0 and 24 h were divided into two groups with significant separation trends, indicating that the metabolite profiles of planktonic MRSA and MRSA biofilms were significantly different. The metabolite profiles of the AS-treated group were significantly separated from those of the 24 h control group, indicating a significant effect of AS on perturbing the metabolism of MRSA biofilms.

Changes in Endogenous-Terminal Small-Molecule Metabolites Before and After the Formation of MRSA Biofilms

Twenty-seven differentially altered metabolites were identified in the two control groups before and after biofilm formation (**Table 2**). These metabolites reflect the metabolic phenotypic characteristics of MRSA biofilm formation. The metabolic pathway analysis showed that phenylalanine, tyrosine, and tryptophan biosynthesis and taurine and hypotaurine metabolism were related to these metabolites ($p < 0.05$) (**Figure 7A**).

Effect of Andrographolide Sulfonate on Endogenous-Terminal Small-Molecule Metabolites in MRSA Biofilms

When biofilms matured, twenty differentially altered metabolites were detected in the MRSA strain from the 25 mg/ml AS-treated group compared with those of the control group (**Table 3**). These metabolites reflected the pharmacodynamic characteristics of 25 mg/ml AS-treated MRSA biofilms and were related to the two most significant pathways, glyoxylate and dicarboxylate metabolism and fatty acid degradation (**Figure 7B**).

Five common terminal metabolites, anthranilic acid, *D*-lactic acid (*D*-LA), kynurenine (KYN), *L*-homocitrulline, and sebacic acid, were identified in the control group and AS group (**Table 4**). Their levels increased during biofilm formation but decreased significantly after treatment with 25 mg/ml AS.

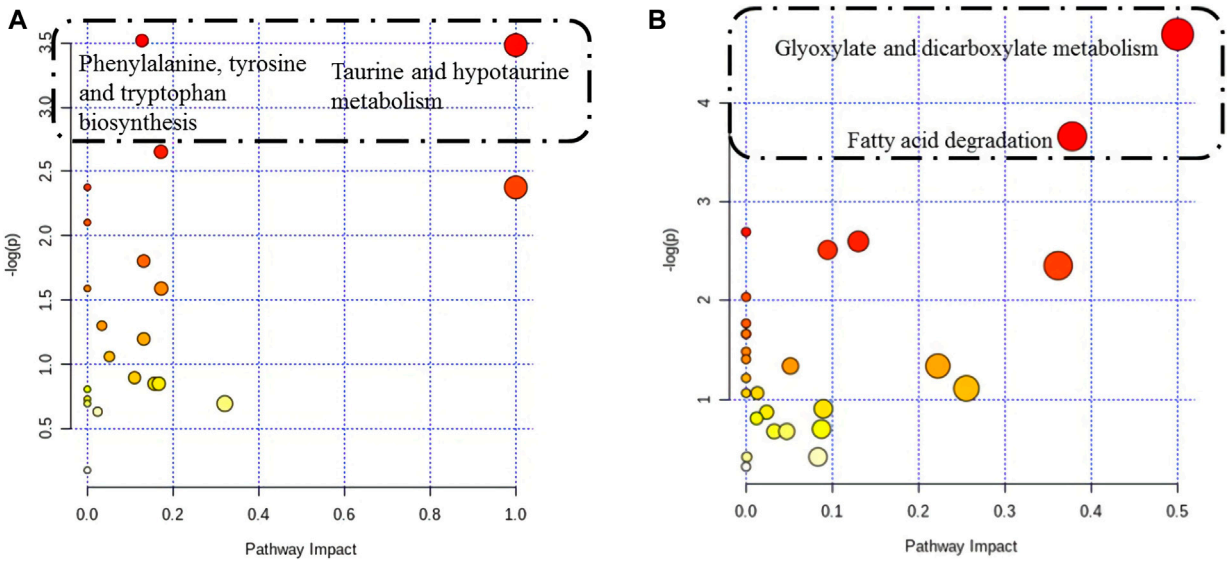

FIGURE 7 | Pathway analysis of differentially altered metabolites in MRSA. **(A)** Overview of the pathway analysis of the 27 biofilm biomarkers. **(B)** Overview of the pathway analysis of the pharmaceutical markers of MRSA biofilms treated with 25 mg/ml AS. The pathway analysis of metabolites with significant differences was performed using MetaboAnalyst 3.0. The bubble chart of the pathway enrichment analysis shows all matched pathways according to the pathway impact values (*X*-axis) of the topological analysis and *p*-values (*Y*-axis) of the pathway enrichment analysis. Each node represents a biological pathway. The bubble area (radius) is proportional to the impact value of each pathway, with the color denoting the significance from the highest in red to the lowest in white. The nodes in the dashed box represent the biological pathways that are significantly related to biofilm markers.

TABLE 3 | Characteristics of terminal metabolites in MRSA biofilms treated with 25 mg/ml AS.

n	R.T (min)	Exact mass	Formula	Compound	KEGG	Fold change
1	1.03	206.0427	$C_7H_{10}O_7$	2-Methylcitric acid	C02225	−3.792
2	N/A	120.0245	$C_4H_8O_2S$	3-(Methylthio)propionic acid	C08276	−6.704
3	N/A	853.152	$C_{25}H_{42}N_7O_{18}P_3S$	3-Hydroxy-2-methylpropanoyl-coenzyme A	C04047	−9.042
4	3.71	809.1258	$C_{23}H_{38}N_7O_{17}P_3S$	Acetyl-coenzyme A	C00024	10.427
5	0.79	137.0477	$C_7H_7NO_2$	Anthranilic acid	C00108	−4.071
6	0.84	192.027	$C_6H_8O_7$	Citric acid	C00158	−3.894
7	4.19	921.251	$C_{31}H_{54}N_7O_{17}P_3S$	Decanoyl-coenzyme A	C05274	−5.859
8	8.19	301.2981	$C_{18}H_{39}NO_2$	*D*-Erythro-dihydrosphingosine	C00836	7.378
9	0.72	90.0317	$C_3H_6O_3$	*D*-Lactic acid	C00256	−3.451
10	5.1	588.2948	$C_{33}H_{40}N_4O_6$	*D*-Urobilin	C05795	−6.841
11	4	1,061.407	$C_{41}H_{74}N_7O_{17}P_3S$	Eicosanoyl-coenzyme A	C02041	5.026
12	5.54	207.0895	$C_{11}H_{13}NO_3$	Homocitrulline	C02427	−4.92
13	0.28	268.0808	$C_{10}H_{12}N_4O_5$	Inosine	C00294	−8.471
14	6.05	189.0426	$C_{10}H_7NO_3$	Kynurenic acid	C01717	−13.006
15	5.41	208.0848	$C_{10}H_{12}N_2O_3$	Kynurenine	C01718	−7.402
16	1.6	105.0426	$C_3H_7NO_3$	*L*-Serine	C00065	−3.434
17	4.45	977.3136	$C_{35}H_{62}N_7O_{17}P_3S$	Myristoyl-coenzyme A	C02593	−12.865
18	0.9	202.1205	$C_{10}H_{18}O_4$	Sebacic acid	C08277	−13.467
19	1.95	379.2488	$C_{18}H_{38}NO_5P$	Sphingosine-1-phosphate	C06124	−9.565
20	1.07	342.1162	$C_{12}H_{22}O_{11}$	Sucrose	C00089	−7.884

DISCUSSION

The treatment of MRSA infection has become a clinically difficult problem. Biofilm formation plays a key role in MRSA infection because the formation of the biofilm provides increased protection of bacteria from antibiotics and host defenses (Chao et al., 2017). Therefore, interfering with the formation of biofilms would be a sensible approach when developing a new treatment for recalcitrant MRSA infections. Currently, the extracts of traditional medicine have become a research hotspot in the development of new antimicrobials. The antibacterial activity of andrographolide, the active component of AG, has been widely studied (Zhang et al., 2019b). However, the absolute bioavailability of AG was reported to be only 2.67%

TABLE 4 | Common terminal metabolites reflecting biofilm formation and AS efficacy.

n	Compound	KEGG	Fold change	
			Control	25 mg/ml AS
1	Anthranilic acid	C00108	6.859	−4.071
2	*D*-Lactic acid	C00256	4.197	−3.451
3	Kynurenine	C01718	3.41	−7.402
4	*L*-Homocitrulline	C02427	3.616	−4.92
5	Sebacic acid	C08277	3.932	−13.467

according to a previous study, which substantially limits its clinical efficacy due to its poor water solubility and susceptibility to extracellular excretion by P-glycoprotein (Ye et al., 2011). By transforming hydroxyl groups into sulfate, the sulfation reaction is an effective method to obtain soluble derivatives with both improved water solubility and bioavailability. The main ingredient of Xiyanping injection is AS, which is modified by AG sulfonation. Several pharmacokinetic studies have shown that AS has a long $t_{1/2}$ (drug half-life), shows considerable metabolic stability, and is rapidly absorbed and distributed to the kidney, colon, liver, and lung tissues (Chong et al., 2013; Lan et al., 2013; Zheng et al., 2016). Safety studies of AS are of equal clinical interest. Only a few randomized occurrences of immediate hypersensitivity reactions to Xiyanping have been reported. A 2017 clinical report cited a 0.12% incidence of adverse reactions following Xiyanping injection (Zhao et al., 2017). Computer analyses of ligand–protein interactions also indicate a very low risk of potential allergic reactions to AS (Yang et al., 2019). The excellent efficacy performance of AS in the treatment of biofilm-mediated infections is under close scrutiny in current anti-infective research (Jiang et al., 2009; Simoes et al., 2009; Ordonez et al., 2011). Nevertheless, the mechanisms underlying the inhibitory effect of AS on MRSA biofilms are still not completely understood. Hence, the therapeutic effect of AS and the precise underlying mechanisms must be elucidated to facilitate the clinical application of AS in the treatment of MRSA infection. We are the first group to document the inhibitory effect of AS on MRSA biofilms and discover the terminal metabolites of the corresponding mechanism through metabolomics. In our experiments, biofilms of MRSA strains isolated from the clinic and MRSA broth supplemented with AS and Van, respectively, were formed *in vitro* after a 24 h incubation of bacteria in the LB medium at room temperature. The expression of genes associated with virulence factors and biofilms was measured using RT-PCR to reveal the association between changes in gene expression and MRSA biofilm formation and AS efficacy. The pharmaceutical mechanisms of AS were identified by performing metabolomics profiling of the corresponding metabolites. Due to the characteristics of TM working mechanisms, metabolomics is particularly suitable for pharmacodynamic studies. Small-molecule metabolites play an important role in biological systems and represent attractive candidates to understand the phenotypes of drug effects. In particular, highly sensitive and specific terminal biomarkers in MRSA biofilms are very useful for a comprehensive study of the efficacy of TM. Therefore, in the present study, a metabolomics approach was employed to determine the subtle change in the metabolite profile of the AS intervention group, explore pharmaceutical biomarkers, and reveal the underlying mechanisms. Meanwhile, the metabolic networks and pathways involved were subjected to KEGG analyses.

In vitro experiments showed a substantial difference in the effective MIC of AS for MRSA compared with Van. Compared with the traditional antibiotic, Van, a higher dose of AS is required to kill planktonic MRSA. However, MRSA can exist in both the planktonic form and biofilms, with the latter being predominant in clinical practice (McCarthy et al., 2015). The formation of biofilms contributes to the ineffective eradication of MRSA infection. When bacteria produce dense biofilms, the situation changes considerably. Matrix components such as PIA and extracellular DNA (eDNA) on the biofilms are important for the bacteria to evade the host immune response and antibiotic attack (Harapanahalli et al., 2015). In the inhibition experiment of AS against MRSA biofilms, only 1/2 MIC of AS inhibited MRSA biofilms. Overall, AS showed a greater advantage in inhibiting MRSA biofilms than planktonic MRSA. In addition, the inhibitory effect was concentration dependent. This discovery extends the general understanding of the antibacterial activity of TM. Our hypothesis that when MRSA biofilms are exposed to the MIC of Van and 1/2 MIC of AS, the 1/2 MIC of AS will cause more significant changes in the physical properties and function of MRSA biofilms and inhibit their growth was confirmed both in biofilm permeation experiments and morphological observations. In addition, SEM showed that AS not only reduced the content of MRSA biofilms but also interfered with the normal cell division of MRSA. This compound inhibited the proliferation of MRSA to a certain extent. However, the specific mechanism requires further studies.

The MRSA biofilm is a microbial colony with a complete structure. The formation of biofilms involves four stages, adhesion, aggregation, maturation, and diffusion, and the process is regulated by virulence factors, regulatory factors, and the QS system. We detected the expression of related genes in planktonic MRSA and mature MRSA biofilms. Notably, sets of genes were upregulated during biofilm formation, namely, *fnbB*, *icaD,* and *PIA*, which mainly contained some known key genes related to adhesion. These key genes may distinguish the biofilm from planktonic MRSA.

The key to the pathogenesis of *Staphylococcus aureus* (*S. aureus*) is its adhesion to host cells and components in the host extracellular matrix (Johannessen et al., 2012). The *S. aureus* genome encodes more than 20 adhesins that mediate initial biofilm cell attachment and intercellular adhesion during biofilm maturation, such as microbial surface component–recognizing adhesion matrix molecules (MSCRAMMs), including surface proteins such as fibronectin-binding proteins A and B (FnbA and FnbB), *clfA*, and *clfB* (Tristan et al., 2003) (Heilmann, 2011). MSCRAMMs have similar structures, with two adjacent IgG fold domains mediating their attachment to host extracellular matrix components such as collagen, fibrinogen, or fibronectin

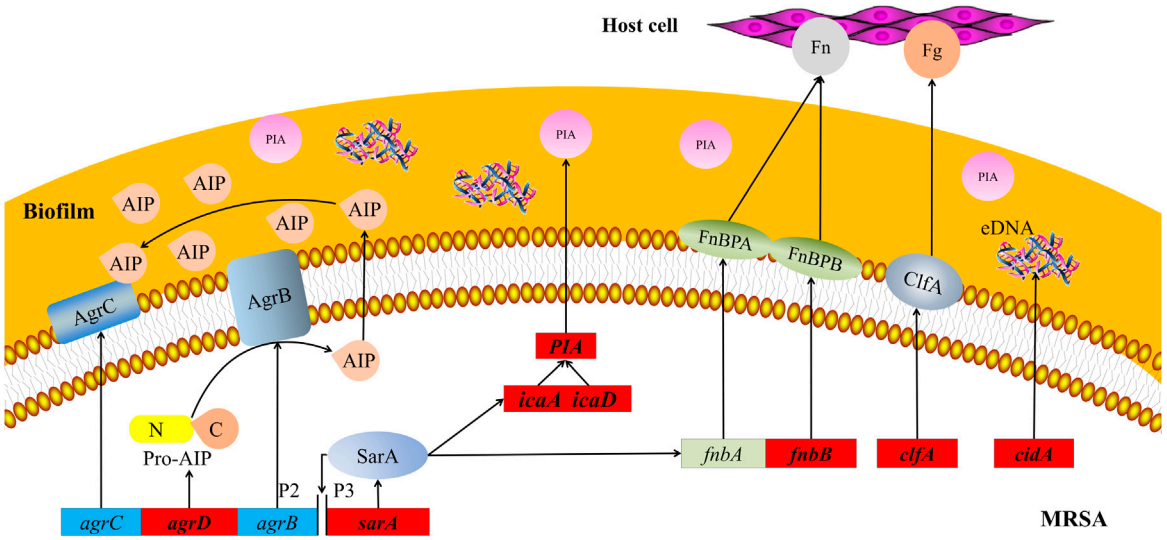

FIGURE 8 | Schematic map of pathways related to MRSA biofilms. Red boxes represent MRSA genes that are downregulated by treatment with 25 mg/ml AS. *agrB*, *agrC,* and *agrD*, accessory gene regulators B, C, and D; AIP, autoinducer peptide; *clfA* and *clfB*, clumping factors A and B; eDNA, extracellular DNA; Fg, fibrinogen; Fn, fibronectin; FnbA and FnbB, fibronectin-binding proteins A and B; *icaA* and *icaD*, intercellular adhesion A and D; MRSA, methicillin-resistant *Staphylococcus aureus*; P2 and P3, promoters 2 and 3; PIA, polysaccharide intercellular adhesion; and *sarA*, staphylococcal accessory regulator.

(**Figure 8**) (Foster et al., 2014). This binding ability is closely related to the pathogenicity of *Staphylococcus aureus* because its adhesion to the extracellular matrix or plasma proteins is a key step in the formation of biofilms. This finding is consistent with the increase in *fnbB* expression detected in our study. *clfA* is the major staphylococcal fibrinogen-binding protein, and its upregulation is responsible for the aggregation of *S. aureus* in the plasma, ultimately leading to arthritis and endocarditis (Foster, 2005).

Molecular studies have shown that during late phases of adherence, organisms first adhere to each other and then elaborate on a biofilm. This step is mediated by two biofilm components, PIA and the intracellular adhesion genes *icaA* and *icaD* (**Figure 8**) (Atshan et al., 2012). These genes are necessary for the synthesis of capsular polysaccharides/adhesion, which are regarded as the major components of MRSA biofilms (Chaieb et al., 2005). PIA is an important component of extracellular matrix–intercellular adhesion and is a key molecule that promotes bacterial cell adhesion (Mack et al., 1996; Vuong et al., 2004). Synthesis of the capsular polysaccharide is mediated by the *ica* operon. Upon activation of this operon, a polysaccharide intercellular adhesin is synthesized. This protein supports cell-to-cell bacterial contacts in a multilayered biofilm. The polysaccharide intercellular adhesin is composed of linear β-1, 6-linked glucosaminylglycans. They are synthesized *in vitro* from UDP-N-acetylglucosamine by the enzyme N-acetylglucosaminyltransferase, which is encoded by the *ica* locus, in particular by the *icaA* gene. The expression of *icaA* alone induces only low enzymatic activity, but coexpression of *icaA* with *icaD* leads to a significant increase in activity and is related to full phenotypic expression of the capsular polysaccharide (Gerke et al., 1998). Therefore, the inhibitory effect of AS on MRSA biofilms may be achieved by inhibiting bacterial adhesion.

The synthesis of virulence factors and other extracellular proteins of *S. aureus* is controlled by the QS system. In MRSA, the QS system is an *agr* system based on the autoinducer peptide (AIP) (**Figure 8**). The pre-AIP of *agr* is encoded by *agrD* and then processed into mature AIP by the membrane protein *agrB* and secreted out of the cell. *agrC* is a membrane receptor kinase that phosphorylates and activates *agrA* after binding to AIP. *agrA* regulates the expression of a series of downstream genes by binding promoter 2 (P2) and promoter 3 (P3). The RNAII transcription frame starting at P2 includes the *agr* locus containing the *agrA*, *agrB*, *agrC,* and *agrD* genes, and the RNAIIItranscription frame starting at P3 is an effector molecule of the *agr* system, encoding virulence factors such as α-hemolysin and δ-toxin (Asad and Opal, 2008). Researchers have speculated that AS inhibits the *agr* system of MRSA by interfering with the activity of *agrD*-encoding AIP, consistent with our RT-PCR results.

sarA is an important regulator of the QS system that positively regulates the production of biofilms and directly regulates the expression of several virulence factors in *S. aureus* (Zielinska et al., 2011; Sina et al., 2013). This protein is an important cause of the pathogenicity and recurrent infection of MRSA. The mechanism by which *sarA* positively regulates biofilms is its inhibition of extracellular enzymes (proteases and nucleases) (Abdelhady et al., 2014). The regulation of virulence factors by *sarA* is mediated by the binding of *sarA*-encoded proteins to peptides encoded in the upstream region, regulating the activation of P2 and P3 (**Figure 8**). P2 regulates the *agr* system through its own induction mechanism. P3 inhibits the

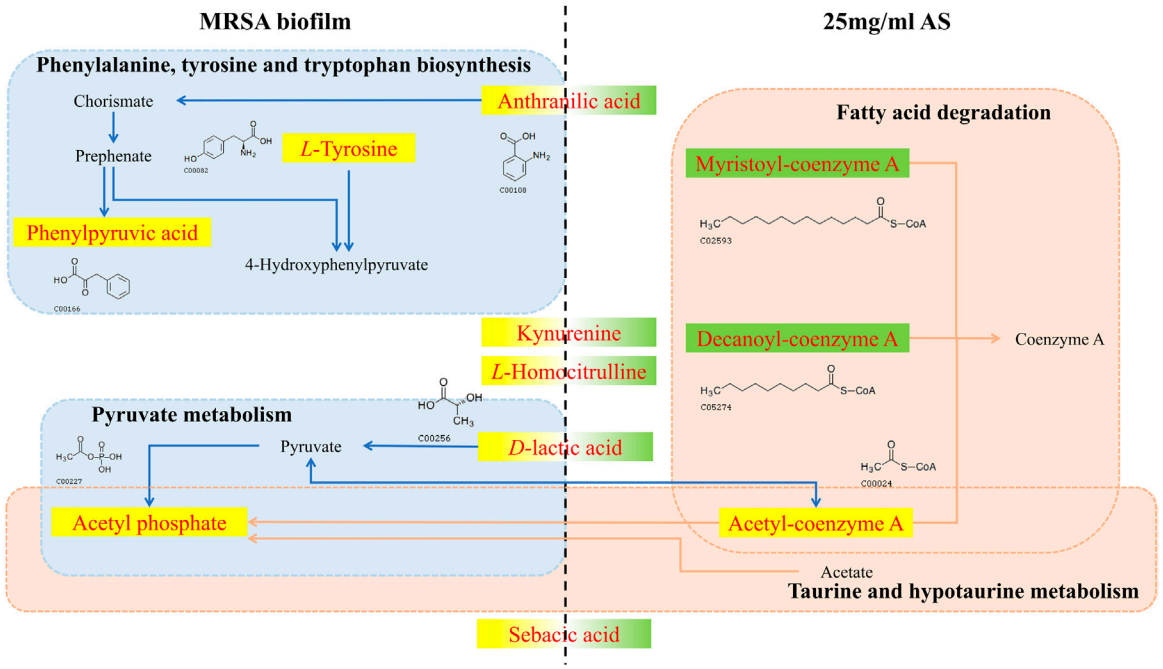

FIGURE 9 | Changes in different metabolites and their metabolic pathways in MRSA biofilms treated with or without AS. The red font indicates the differentially altered metabolite in the pathway. The yellow background indicates that the level of the metabolite increased, and the green background indicates a decrease. The blue dashed boxes indicate pathways in which metabolic biomarkers of the MRSA biofilm are involved in the absence of the intervention. Pink dashed boxes indicate pathways in which pharmacodynamic metabolic markers of AS are involved.

production of biofilms and induces the expression of virulence factors by regulating the production of RNAIII (Blasi et al., 2016; Roy et al., 2018). In our experiment, the transcription of *sarA* was significantly downregulated after the AS intervention. This result is consistent with previous findings that AG (the parent compound of AS) significantly inhibits *sarA* activity. Therefore, AS exhibits antibiofilm and antivirulence activities by inhibiting *sarA* gene expression.

cidA is an important regulatory factor involved in the formation of *S. aureus* biofilms. The expression of *cidA* is related to bacterial adhesion and genomic DNA release and is continuously upregulated during biofilm formation (**Figure 8**) (Grande et al., 2014). The cid/LGR holin–antiholin system is related to the release of eDNA during cell lysis and planktonic growth, and it promotes adhesion and biofilm formation (Rice et al., 2007). eDNA, an important component of the extracellular polymer matrix, plays an important role in determining the stability and development of biofilms and is widely involved in the regulation of the formation of Gram-positive bacterial biofilms (Spoering and Gilmore, 2006). Activation of trichourea hydrolase contributes to the release of eDNA from biofilms (Bose et al., 2012). The protein encoded by *cidA* increases the activity of trichourea hydrolase and promotes bacterial separation from biofilms and dissemination to new infection sites (Ranjit et al., 2011). Researchers have suggested a potential role of *cidA* in the stage of biofilm adhesion or diffusion. Based on the results of the present study, the expression of *cidA* was significantly downregulated after the intervention of 25 mg/ml AS, suggesting that AS may inhibit the expression of eDNA regulated by *cidA* in the stage of biofilm adhesion or diffusion.

In the process by which AS interferes with the formation of MRSA biofilms, AS significantly induced changes in the level of five metabolites, namely, anthranilic acid, KYN, *L*-homocitrulline, *D*-LA, and sebacic acid (**Figure 9**). Alterations in these metabolites might be responsible for the common formation of MRSA biofilms or therapeutic effects of drugs. Anthranilic acid is a key node in a complex pathway required for the synthesis of several important secondary metabolites in *Pseudomonas aeruginosa* (*P. aeruginosa*) (Vital-Lopez et al., 2015). Anthranilic acid facilitates the attachment of cells to the surface in the early stage of biofilm development. In addition, it affects the transcription of extracellular polymeric substance (EPS) operons. *P. aeruginosa* contains three major EPSs in the biofilm matrix: Psl, Pel, and alginate. Anthranilic acid treatment increases the transcription of the Psl operon by 85% (Vital-Lopez et al., 2015). Therefore, we speculate that AS inhibits the formation of biofilms by inhibiting anthranilic acid production in MRSA to affect cell adhesion and EPS production. KYN, the precursor of anthranilic acid, is critical for *P. aeruginosa* virulence. This bacterium utilizes multiple QS pathways to coordinate an arsenal of virulence factors. The kynurenine pathway (KP) has been implicated in the QS and virulence factor expression (Kasper et al., 2016). The downregulation of KYN levels may be related to the effect of the AS intervention on the transcription of QS-related genes

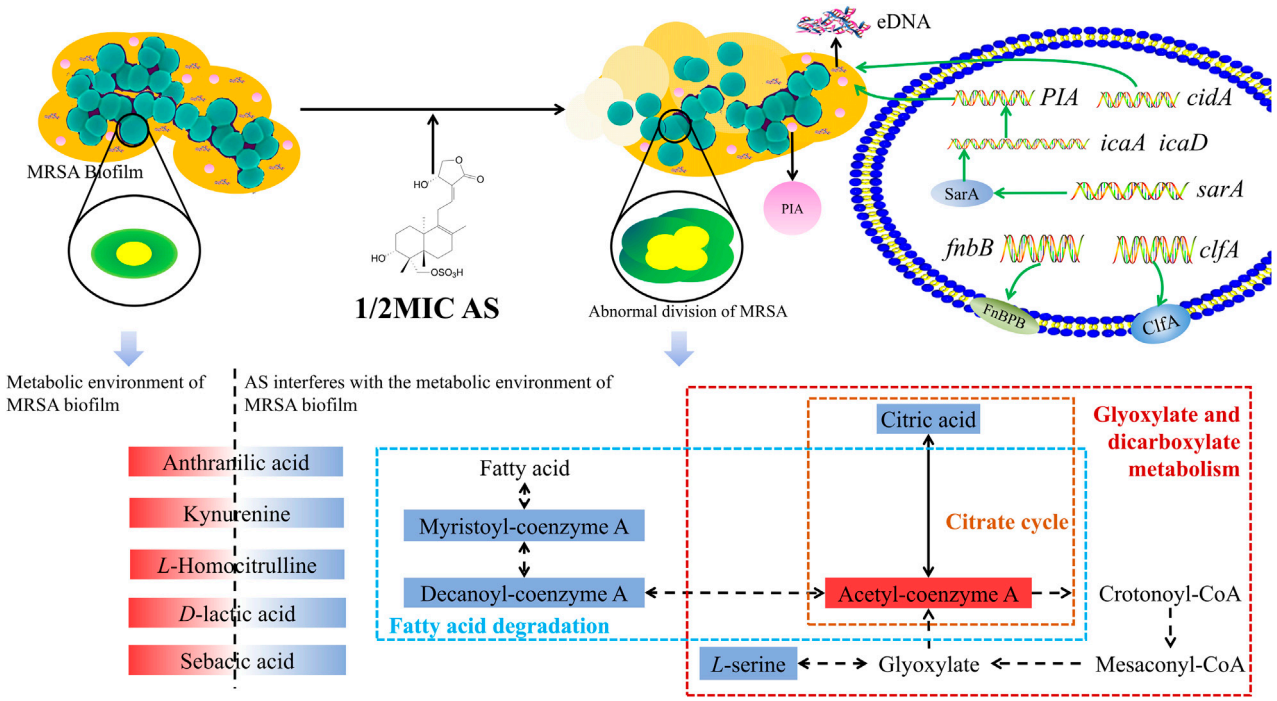

FIGURE 10 | Overview of the technical analyses described in the article. eDNA, extracellular DNA; PIA, polysaccharide intercellular adhesion; *icaA*, intercellular adhesion A; *icaD*, intercellular adhesion D; and FnbB, fibronectin-binding protein B. The red solid box represents upregulated metabolite levels, and the blue box represents the downregulated levels. The blue dashed box represents the fatty acid degradation pathway, the yellow dashed box represents the citrate cycle pathway, and the red box represents glyoxylate and dicarboxylate metabolism.

(*agrD* and *sarA*). *D*-LA, a natural organic acid, is an important carbon and energy source for pathogens and commensal bacteria in mammalian hosts (Jiang et al., 2014; Gillis et al., 2018; Lin et al., 2018). In addition, *D*-LA can be used as an electron donor for aerobic respiration in the upper, oxic portion of the biofilm (Lin et al., 2018). *P. aeruginosa* is the most common cause of chronic, biofilm-based lung infections in patients with cystic fibrosis (CF). The lung environment of patients with CF might nevertheless contain subregions where lactate is a major source of carbon and energy (Lin et al., 2018). Furthermore, PA14 has the potential to utilize *D*-LA during growth in colony biofilms (Lin et al., 2018). Thus, the increased level of *D*-LA may play a positive role in promoting biofilm formation by providing an energy source. The downregulation of *D*-LA may contribute to AS-induced decreases in the carbon and energy sources needed for the growth of the MRSA biofilm and subsequent damage.

Phenylpyruvic acid, *D*-2-aminobutyric acid, and *L*-tyrosine are characteristic metabolites involved in the formation of MRSA biofilms. Treatment with 25 mg/ml AS did not alter the levels of these metabolites. Phenylpyruvic acid is formed by the decomposition of phenylalanine into *L*-tyrosine (Wang et al., 2017). Phenylpyruvic acid is involved in the metabolism of amino acids during the formation of MRSA biofilms. *D*-2-Aminobutyric acid, an unnatural amino acid, enhances the activity of phosphatase, which can hydrolyze phosphate ester and polyphosphoric acid compounds. *D*-2-Aminobutyric acid levels decrease in the process of biofilm formation, ensuring the formation of phosphoteichoic acid as a cell wall component. By performing a metabolite pathway analysis, these metabolites were found to be involved in the biosynthesis of phenylalanine, tyrosine, and tryptophan, as well as in taurine and hypotaurine metabolism. These two metabolic pathways may significantly affect the formation of MRSA biofilms. D-Urobilin, decanoyl-coenzyme A, myristoyl-coenzyme A, and acetyl-coenzyme A are biomarkers reflecting the therapeutic effect of AS. The metabolic pathway analysis showed that glyoxylate and dicarboxylate metabolism and fatty acid degradation were the most significant pathways of terminal metabolites reflecting the therapeutic effect of AS.

CONCLUSIONS

MRSA biofilms are one of the causes of antibiotic resistance, and their formation can be inhibited by AS. AS not only inhibits the survival of MRSA in the biofilms but also inhibits the proliferation of MRSA by interfering with cell division. Its mechanism is mediated by downregulating the transcription of genes related to the QS system, bacterial adhesion, and eDNA release and interfering with the amino acid, fatty acid, taurine, and secondary taurine metabolism in MRSA (**Figure 10**). This

study provides a theoretical foundation for the application of AS as an anti-MRSA biofilm agent.

DATA AVAILABILITY STATEMENT

The datasets presented in this study can be found in online repositories. The names of the repository/repositories and accession number(s) can be found in the article.

AUTHOR CONTRIBUTIONS

LZ and BW contributed equally to this work and should be considered the co-first authors. YT, CL, and WY conceived the experiments. LZ and MB conducted the experiments. YC, QC, and LLv analyzed the results. BW, LLi, and NX prepared the figure. LZ and BW wrote the main manuscript text. JY, CL, TM, YT, and WY wrote the review and did final editing. All the authors contributed to critical scrutiny of the literature and its approval.

FUNDING

This work was supported by the National Science and Technology Major Project (2017YFC1703701); the Fundamental Research Funds for the Central Public Welfare Research Institutes (Z0653, Z0656); the Beijing TCM Science and Technology Development Fund Project (JJ2018-102); the CACMS Innovation Fund (CI2021A00704-2); the Open Project of the State Key Laboratory of Innovative Natural Medicine and TCM Injections (QFSKL2018003); the International Cooperation of China Academy of Chinese Medical Sciences (GH201909).

REFERENCES

Abdelhady, W., Bayer, A. S., Seidl, K., Moormeier, D. E., Bayles, K. W., Cheung, A., et al. (2014). Impact of Vancomycin on sarA-Mediated Biofilm Formation: Role in Persistent Endovascular Infections Due to Methicillin-Resistant *Staphylococcus aureus*. *J. Infect. Dis.* 209, 1231–1240. doi:10.1093/infdis/jiu007

Anderl, J., Franklin, M., and Stewart, P. (2000). Role of Antibiotic Penetration Limitation in Klebsiella pneumoniae Biofilm Resistance to Ampicillin and Ciprofloxacin. *Antimicrob. Agents Chemother.* 44, 1818–1824. doi:10.1128/aac.44.7.1818-1824.2000

Asad, S., and Opal, S. M. (2008). Bench-to-bedside Review: Quorum Sensing and the Role of Cell-To-Cell Communication during Invasive Bacterial Infection. *Crit. Care* 12, 236. doi:10.1186/cc7101

Atshan, S. S., Nor Shamsudin, M., Sekawi, Z., Lung, L. T. T., Hamat, R. A., Karunanidhi, A., et al. (2012). Prevalence of Adhesion and Regulation of Biofilm-Related Genes in Different Clones of Staphylococcus Aureus. *J. Biomed. Biotechnol.* 2012, 1–10. doi:10.1155/2012/976972

Banerjee, M., Parai, D., Chattopadhyay, S., and Mukherjee, S. K. (2017). Andrographolide: Antibacterial Activity against Common Bacteria of Human Health Concern and Possible Mechanism of Action. *Folia Microbiol.* 62, 237–244. doi:10.1007/s12223-017-0496-9

Blasi, F., Page, C., Rossolini, G. M., Pallecchi, L., Matera, M. G., Rogliani, P., et al. (2016). The Effect of N-acetylcysteine on Biofilms: Implications for the Treatment of Respiratory Tract Infections. *Respir. Med.* 117, 190–197. doi:10.1016/j.rmed.2016.06.015

Borges, A., Saavedra, M., and Simoes, M. (2015). Insights on Antimicrobial Resistance, Biofilms and the Use of Phytochemicals as New Antimicrobial Agents. *Cmc* 22, 2590–2614. doi:10.2174/0929867322666150530210522

Bose, J. L., Lehman, M. K., Fey, P. D., and Bayles, K. W. (2012). Contribution of the *Staphylococcus aureus* Atl AM and GL Murein Hydrolase Activities in Cell Division, Autolysis, and Biofilm Formation. *PLoS One* 7, e42244. doi:10.1371/journal.pone.0042244

Cascioferro, S., Carbone, D., Parrino, B., Pecoraro, C., Giovannetti, E., Cirrincione, G., et al. (2021). Therapeutic Strategies to Counteract Antibiotic Resistance in MRSA Biofilm-Associated Infections. *ChemMedChem* 16, 65–80. doi:10.1002/cmdc.202000677

Castillo-Juárez, I., Maeda, T., Mandujano-Tinoco, E. A., Tomás, M., Pérez-Eretza, B., García-Contreras, S. J., et al. (2015). Role of Quorum Sensing in Bacterial Infections. *Wjcc* 3, 575–598. doi:10.12998/wjcc.v3.i7.575

Chaieb, K., Mahdouani, K., and Bakhrouf, A. (2005). Detection of icaA and icaD Loci by Polymerase Chain Reaction and Biofilm Formation by Staphylococcus Epidermidis Isolated from Dialysate and needles in a Dialysis Unit. *J. Hosp. Infect.* 61, 225–230. doi:10.1016/j.jhin.2005.05.014

Chao, Y., Bergenfelz, C., and Håkansson, A. P. (2017). *In Vitro* and *In Vivo* Biofilm Formation by Pathogenic Streptococci. *Methods Mol. Biol.* 1535, 285–299. doi:10.1007/978-1-4939-6673-8_19

Cheung, A. L., Bayer, M. G., and Heinrichs, J. H. (1997). Sar Genetic Determinants Necessary for Transcription of RNAII and RNAIII in the Agr Locus of *Staphylococcus aureus*. *J. Bacteriol.* 179, 3963–3971. doi:10.1128/jb.179.12.3963-3971.1997

Chong, L., Chen, W., Luo, Y., and Jiang, Z. (2013). Simultaneous Determination of 9-dehydro-17-hydro-andrographolide and Sodium 9-dehydro-17-hydro-andrographolide-19-yl Sulfate in Rat Plasma by UHPLC-ESI-MS/MS after Administration of Xiyanping Injection: Application to a Pharmacokine. *Biomed. Chromatogr.*. England: Chichester 27, 825-830. doi:10.1002/bmc.2866

Chopra, S., Harjai, K., and Chhibber, S. (2015). Antibiotic Susceptibility of Ica-Positive and Ica-Negative MRSA in Different Phases of Biofilm Growth. *J. Antibiot. (Tokyo)*, 15–22. doi:10.1038/ja.2014.96

Craft, K. M., Nguyen, J. M., Berg, L. J., and Townsend, S. D. (2019). Methicillin-resistant *Staphylococcus aureus* (MRSA): Antibiotic-Resistance and the Biofilm Phenotype. *Med. Chem. Commun.* 10, 1231–1241. doi:10.1039/c9md00044e

Fankam, A. G., Kuete, V., Voukeng, I. K., Kuiate, J. R., and Pages, J.-M. (2011). Antibacterial Activities of Selected Cameroonian Spices and Their Synergistic Effects with Antibiotics against Multidrug-Resistant Phenotypes. *BMC Complement. Altern. Med.* 11, 104. doi:10.1186/1472-6882-11-104

Feng, E., Shen, K., Lin, F., Lin, W., Zhang, T., Zhang, Y., et al. (2020). Improved Osteogenic Activity and Inhibited Bacterial Biofilm Formation on Andrographolide-Loaded Titania Nanotubes. *Ann. Transl Med.* 8, 987. doi:10.21037/atm-20-4901

Foster, T. J., Geoghegan, J. A., Ganesh, V. K., and Höök, M. (2014). Adhesion, Invasion and Evasion: the many Functions of the Surface Proteins of *Staphylococcus aureus*. *Nat. Rev. Microbiol.* 12, 49–62. doi:10.1038/nrmicro3161

Foster, T. J. (2005). Immune Evasion by Staphylococci. *Nat. Rev. Microbiol.* 3, 948–958. doi:10.1038/nrmicro1289

Fulaz, S., Devlin, H., Vitale, S., Quinn, L., O'Gara, J. P., and Casey, E. (2020). Tailoring Nanoparticle-Biofilm Interactions to Increase the Efficacy of Antimicrobial Agents against *Staphylococcus aureus*. *Ijn* 15, 4779–4791. doi:10.2147/IJN.S256227

Gerke, C., Kraft, A., Süßmuth, R., Schweitzer, O., and Götz, F. (1998). Characterization of the N-Acetylglucosaminyltransferase Activity Involved in the Biosynthesis of the Staphylococcus epidermidis Polysaccharide Intercellular Adhesin. *J. Biol. Chem.* 273, 18586–18593. doi:10.1074/jbc.273.29.18586

Gillis, C. C., Hughes, E. R., Spiga, L., Winter, M. G., Zhu, W., Furtado de Carvalho, T., et al. (2018). Dysbiosis-Associated Change in Host Metabolism Generates

Lactate to Support Salmonella Growth. *Cell Host Microbe* 23, 54–64. doi:10.1016/j.chom.2017.11.006

Grande, R., Nistico, L., Sambanthamoorthy, K., Longwell, M., Iannitelli, A., Cellini, L., et al. (2014). Temporal Expression ofagrB, cidA, alsS in the Early Development of Staphylococcus aureus UAMS-1 Biofilm Formation and the Structural Role of Extracellular DNA and Carbohydrates. *Pathog. Dis.* 70, 414–422. doi:10.1111/2049-632X.12158

Harapanahalli, A. K., Chen, Y., Li, J., Busscher, H. J., and van der Mei, H. C. (2015). Influence of Adhesion Force on icaA and cidA Gene Expression and Production of Matrix Components in *Staphylococcus aureus* Biofilms. *Appl. Environ. Microbiol.* 81, 3369-3378. doi:10.1128/AEM.04178-14

Heilmann, C. (2011). Adhesion Mechanisms of Staphylococci. *Adv. Exp. Med. Biol.* 715, 105–123. doi:10.1007/978-94-007-0940-9_7

Howden, B. P., Davies, J. K., Johnson, P. D. R., Stinear, T. P., and Grayson, M. L. (2010). Reduced Vancomycin Susceptibility in *Staphylococcus aureus*, Including Vancomycin-Intermediate and Heterogeneous Vancomycin-Intermediate Strains: Resistance Mechanisms, Laboratory Detection, and Clinical Implications. *Clin. Microbiol. Rev.* 23, 99–139. doi:10.1128/CMR.00042-09

Jiang, T., Gao, C., Ma, C., and Xu, P. (2014). Microbial Lactate Utilization: Enzymes, Pathogenesis, and Regulation. *Trends Microbiol.* 22, 589–599. doi:10.1016/j.tim.2014.05.008

Jiang, X., Yu, P., Jiang, J., Zhang, Z., Wang, Z., Yang, Z., et al. (2009). Synthesis and Evaluation of Antibacterial Activities of Andrographolide Analogues. *Eur. J. Med. Chem.* 44, 2936–2943. doi:10.1016/j.ejmech.2008.12.014

Johannessen, M., Sollid, J. E., and Hanssen, A.-M. (2012). Host- and Microbe Determinants that May Influence the success of *S. aureus* Colonization. *Front. Cel. Inf. Microbio.* 2, 56. doi:10.3389/fcimb.2012.00056

Kasper, S. H., Bonocora, R. P., Wade, J. T., Musah, R. A., and Cady, N. C. (2016). Chemical Inhibition of Kynureninase Reduces *Pseudomonas aeruginosa* Quorum Sensing and Virulence Factor Expression. *ACS Chem. Biol.* 11, 1106–1117. doi:10.1021/acschembio.5b01082

Lan, C., Luo, Y. H., Yang, X. L., Chen, F., and Chen, W. K. (2013). Tissue Distribution of Sodium 9-Dehydro-17-Hydro-Andrographolide-19-Yl Sulfate in Rats *In Vivo*. *Chinese Traditional Patent Medicine*.

Liew, K. Y., Hafiz, M. F., Chong, Y. J., Harith, H. H., Israf, D. A., and Tham, C. L. (2020). A Review of Malaysian Herbal Plants and Their Active Constituents with Potential Therapeutic Applications in Sepsis. *Evid. Based Complement. Alternat Med.* 2020, 8257817. doi:10.1155/2020/8257817

Lin, Y.-C., Cornell, W. C., Jo, J., Price-Whelan, A., and Dietrich, L. E. P. (2018). The *Pseudomonas aeruginosa* Complement of Lactate Dehydrogenases Enables Use of D - and L -Lactate and Metabolic Cross-Feeding. *mBio* 9. doi:10.1128/mBio.00961-18

Mack, D., Haeder, M., Siemssen, N., and Laufs, R. (1996). Association of Biofilm Production of Coagulase-Negative Staphylococci with Expression of a Specific Polysaccharide Intercellular Adhesin. *J. Infect. Dis.* 174, 881–883. doi:10.1093/infdis/174.4.881

McCarthy, H., Rudkin, J. K., Black, N. S., Gallagher, L., O'Neill, E., and O'Gara, J. P. (2015). Methicillin Resistance and the Biofilm Phenotype in *Staphylococcus aureus*. *Front. Cel. Infect. Microbiol.* 5, 1. doi:10.3389/fcimb.2015.00001

McGuinness, W. A., Malachowa, N., and DeLeo, F. R. (2017). Vancomycin Resistance in *Staphylococcus aureus*. *Yale J. Biol. Med.* 90, 269–281. Available at: https://www.ncbi.nlm.nih.gov/pubmed/28656013.

Ordóñez, P. E., Quave, C. L., Reynolds, W. F., Varughese, K. I., Berry, B., Breen, P. J., et al. (2011). Sesquiterpene Lactones from Gynoxys Verrucosa and Their Anti-MRSA Activity. *J. Ethnopharmacology* 137, 1055–1059. doi:10.1016/j.jep.2011.07.012

Patil, R., and Jain, V. (2020). Andrographolide: A Review of Analytical Methods. *J. Chromatogr. Sci.*. doi:10.1093/chromsci/bmaa091

Ranjit, D. K., Endres, J. L., and Bayles, K. W. (2011). *Staphylococcus aureus* CidA and LrgA Proteins Exhibit Holin-like Properties. *J. Bacteriol.* 193, 2468–2476. doi:10.1128/JB.01545-10

Rice, K. C., Mann, E. E., Endres, J. L., Weiss, E. C., Cassat, J. E., Smeltzer, M. S., et al. (2007). The cidA Murein Hydrolase Regulator Contributes to DNA Release and Biofilm Development in *Staphylococcus aureus*. *Proc. Natl. Acad. Sci.* 104, 8113–8118. doi:10.1073/pnas.0610226104

Roy, R., Tiwari, M., Donelli, G., and Tiwari, V. (2018). Strategies for Combating Bacterial Biofilms: A Focus on Anti-biofilm Agents and Their Mechanisms of Action. *Virulence* 9, 522–554. doi:10.1080/21505594.2017.1313372

Shi, H., Guo, W., Zhu, H., Li, M., Ung, C. O. L., Hu, H., et al. (2019). Cost-Effectiveness Analysis of Xiyanping Injection (Andrographolide Sulfonate) for Treatment of Adult Community Acquired Pneumonia: A Retrospective, Propensity Score-Matched Cohort Study. *Evidence Based Complementary & Alternative Medicine Ecam* 2019, 4510591. doi:10.1155/2019/4510591

Simoes, M., Bennett, R. N., and Rosa, E. A. (2009). Understanding Antimicrobial Activities of Phytochemicals against Multidrug Resistant Bacteria and Biofilms. *Nat. Prod. Rep.* 26, 746–757. doi:10.1039/b821648g

Sina, H., Ahoyo, T. A., Moussaoui, W., Keller, D., Bankolé, H. S., Barogui, Y., et al. (2013). Variability of Antibiotic Susceptibility and Toxin Production of *Staphylococcus aureus* Strains Isolated from Skin, Soft Tissue, and Bone Related Infections. *BMC Microbiol.* 13, 188. doi:10.1186/1471-2180-13-188

Solano, C., Echeverz, M., and Lasa, I. (2014). Biofilm Dispersion and Quorum Sensing. *Curr. Opin. Microbiol.* 18, 96–104. doi:10.1016/j.mib.2014.02.008

Spoering, A. L., and Gilmore, M. S. (2006). Quorum sensing and DNA Release in Bacterial Biofilms. *Curr. Opin. Microbiol.* 9, 133–137. doi:10.1016/j.mib.2006.02.004

Sun, T., Li, X.-D., Hong, J., Liu, C., Zhang, X.-L., Zheng, J.-P., et al. (2019). Inhibitory Effect of Two Traditional Chinese Medicine Monomers, Berberine and Matrine, on the Quorum Sensing System of Antimicrobial-Resistant *Escherichia coli*. *Front. Microbiol.* 10, 2584. doi:10.3389/fmicb.2019.02584

Thomas, T., Gilbert, J., and Meyer, F. (2012). Metagenomics - a Guide from Sampling to Data Analysis. *Microb. Inform. Exp* 2, 3. doi:10.1186/2042-5783-2-3

Tristan, A., Ying, L., Bes, M., Etienne, J., Vandenesch, F., and Lina, G. (2003). Use of Multiplex PCR to Identify *Staphylococcus aureus* Adhesins Involved in Human Hematogenous Infections. *J. Clin. Microbiol.* 41, 4465–4467. doi:10.1128/jcm.41.9.4465-4467.2003

Yang, Q.-W., Li, Q., Zhang, J., Xu, Q., Yang, X., et al. (2019). Crystal Structure and Anti-inflammatory and Anaphylactic Effects of Andrographlide Sulphonate E in Xiyanping, a Traditional Chinese Medicine Injection. *J. Pharm. Pharmacol.* 71, 251–259. doi:10.1111/jphp.13028

Vital-Lopez, F. G., Reifman, J., and Wallqvist, A. (2015). Biofilm Formation Mechanisms of *Pseudomonas aeruginosa* Predicted via Genome-Scale Kinetic Models of Bacterial Metabolism. *Plos Comput. Biol.* 11, e1004452. doi:10.1371/journal.pcbi.1004452

Vuong, C., Voyich, J. M., Fischer, E. R., Braughton, K. R., Whitney, A. R., DeLeo, F. R., et al. (2004). Polysaccharide Intercellular Adhesin (PIA) Protects Staphylococcus Epidermidis against Major Components of the Human Innate Immune System. *Cell Microbiol* 6, 269–275. doi:10.1046/j.1462-5822.2004.00367.x

Wang, L.-H., Wang, M.-S., Zeng, X.-A., Xu, X.-M., and Brennan, C. S. (2017). Membrane and Genomic DNA Dual-Targeting of Citrus Flavonoid Naringenin against *Staphylococcus aureus*. *Integr. Biol.* 9, 820–829. doi:10.1039/c7ib00095b

Wang, X., Sun, H., Zhang, A., Sun, W., Wang, P., and Wang, Z. (2011a). Potential Role of Metabolomics Apporoaches in the Area of Traditional Chinese Medicine: as Pillars of the Bridge between Chinese and Western Medicine. *J. Pharm. Biomed. Anal.* 55, 859–868. doi:10.1016/j.jpba.2011.01.042

Wang, Y., Wang, T., Hu, J., Ren, C., Lei, H., Hou, Y., et al. (2011b). Anti-biofilm Activity of TanReQing, a Traditional Chinese Medicine Used for the Treatment of Acute Pneumonia. *J. ethnopharmacology* 134, 165–170. doi:10.1016/j.jep.2010.11.066

Wehrens, R., and Salek, R. M. (2016). *Metabolomics: Practical Guide to Design and Analysis*, CRC Press.

Yang, W., Liu, J., Blažeković, B., Sun, Y., Ma, S., Ren, C., et al. (2018). *In Vitro* antibacterial Effects of Tanreqing Injection Combined with Vancomycin or Linezolid against Methicillin-Resistant *Staphylococcus aureus*. *BMC Complement. Altern. Med.* 18, 169. doi:10.1186/s12906-018-2231-8

Ye, L., Wang, T., Tang, L., Liu, W., Yang, Z., Zhou, J., et al. (2011). Poor Oral Bioavailability of a Promising Anticancer Agent Andrographolide Is Due to Extensive Metabolism and Efflux by P-Glycoprotein. *J. Pharm. Sci.*.

Zhang, G., Jiang, C., Xie, N., Xu, Y., Liu, L., and Liu, N. (2019a). Treatment with Andrographolide Sulfonate Provides Additional Benefits to Imipenem in a Mouse Model of *Klebsiella pneumoniae* Pneumonia. *Biomed. Pharmacother.* 100, 5007–5017. doi:10.1016/j.biopha.2019.10906510.1002/jps.22693

Zhang, L., Bao, M., Liu, B., Zhao, H., Zhang, Y., Ji, X., et al. (2019b). Effect of Andrographolide and its Analogs on Bacterial Infection: a Review. *Pharmacology* 105, 123–134. doi:10.1159/000503410

Zhang, L., Liang, E., Cheng, Y., Mahmood, T., Ge, F., Zhou, K., et al. (2020). Is Combined Medication with Natural Medicine a Promising Therapy for Bacterial Biofilm Infection?. *Biomed. Pharmacother.* 128, 110184. doi:10.1016/j.biopha.2020.110184

Zhang, Y., Li, W., Zou, L., Gong, Y., Zhang, P., Xing, S., et al. (2018). Metabonomic Study of the Protective Effect of Fukeqianjin Formula on Multi-Pathogen Induced Pelvic Inflammatory Disease in Rats. *Chin. Med.* 13, 61. doi:10.1186/s13020-018-0217-6

Zhao, Y., Huang, P., Chen, Z., Zheng, S.-w., Yu, J.-y., and Shi, C. (2017). Clinical Application Analysis of Andrographolide Total Ester Sulfonate Injection,a Traditional Chinese Medicine Licensed in China. *J. Huazhong Univ. Sci. Technol.* 299, 299.

Zheng, D., Shao, J., Chen, W., and Luo, Y. (2016). *In Vitro* Metabolism of Sodium 9-Dehydro-17-Hydro-Andrographolide-19-Yl Sulfate in Rat Liver S9 by Liquid Chromatography-Mass Spectrometry Method. *Pharmacogn Mag.* 12, S102–S108. doi:10.4103/0973-1296.182194

Zielinska, A. K., Beenken, K. E., Joo, H.-S., Mrak, L. N., Griffin, L. M., Luong, T. T., et al. (2011). Defining the Strain-dependent Impact of the Staphylococcal Accessory Regulator (sarA) on the Alpha-Toxin Phenotype of *Staphylococcus aureus*. *J. Bacteriol.* 193, 2948–2958. doi:10.1128/JB.01517-10

Conflict of Interest: LL and NX were employed by Qingfeng Pharmaceutical Co. Ltd, Ganzhou, Jiangxi Province.

The remaining authors declare that the research was conducted in the absence of any commercial or financial relationships that could be construed as a potential conflict of interest.

Publisher's Note: All claims expressed in this article are solely those of the authors and do not necessarily represent those of their affiliated organizations, or those of the publisher, the editors and the reviewers. Any product that may be evaluated in this article, or claim that may be made by its manufacturer, is not guaranteed or endorsed by the publisher.